Applied Catalysis B: Environmental 172–173 (2015) 165–173

Contents lists available at ScienceDirect

Applied Catalysis B: Environmental

journal homepage: www.elsevier.com/locate/apcatb

Superior photocatalytic activities of NiO octahedrons with loaded AgCl particles and charge separation between polar NiO {1 1 1} surfaces

Bin Liu [a], Heqing Yang [a,*], Aihua Wei [a], Hua Zhao [a], Lichao Ning [b], Congjie Zhang [b], Shengzhong Liu [c]

[a] Key Laboratory of Macromolecular Science of Shaanxi Province, School of Materials Science and Engineering, Shaanxi Normal University, Xi'an 710119, China
[b] Key Laboratory of Macromolecular Science of Shaanxi Province, School of Chemistry and Chemical Engineering, Shaanxi Normal University, Xi'an 710119, China
[c] Key Laboratory of Applied Surface and Colloid Chemistry, Ministry of Education, School of Materials Science and Engineering, Shaanxi Normal University, Xi'an 710119, China

ARTICLE INFO

Article history:
Received 12 September 2014
Received in revised form 7 February 2015
Accepted 9 February 2015
Available online 10 February 2015

Keywords:
NiO octahedrons with loaded AgCl particles
Photocatalytic activity
Charge separation
Polar NiO {1 1 1} surfaces

ABSTRACT

Crystal facet engineering of semiconductors is proven to be an effective strategy to increase photocatalytic performances. However, the mechanism involved in the photocatalysis is not yet known. Here, we found that photocatalytic performances of the Cl^- ion capped NiO octahedrons with exposed {1 1 1} facets were activated by treatment of $AgNO_3$ and $NH_3{\cdot}H_2O$ solutions. The clean NiO {1 1 1} facets were found to be highly reactivity faces. Based on polar structure of the {1 1 1} surfaces, a charge separation model between polar {1 1 1} surfaces is proposed. The internal electric field created by the spontaneous polarization drives effectively separation of photogenerated electrons and holes. The reduction and oxidation reactions selectively take place on the positive Ni—NiO and negative O—NiO planes. The good charge separation results in high photocatalytic activity. Our model suggests the polar surface-engineering as a strategy to develop more effective photocatalysts and new type of solar cells, electronic and photoelectric devices.

Published by Elsevier B.V.

1. Introduction

Since the discovery of photoinduced decomposition of water on TiO_2 electrodes semiconductor photocatalysis have attracted worldwide attention for their potentials in environmental and energy applications [1–4]. The reactivity of the photocatalyst is definitely affected by surface atomic arrangement and coordination [5–17]. There have been reports that {0 0 1} facets of anatase TiO_2 [7], $BiVO_4$ [8], BiOCl [9], WO_3 [10], β-Bi_2O_3 [11], CdS [12] and Bi_2WO_6 [13], Ag_3PO_4 {1 1 0} [14] and InOOH {0 2 0} facets [15] as well as Cu_2O {1 1 1} [16] and {5 2 2} facets [17] exhibited enhanced photocatalytic activity for degradation of toxic organic pollutants, splitting of water and reduction of CO_2. However, the mechanism involved in the photocatalysis is not yet known.

Despite the facet that these highly reactive facets are important in improving photocatalytic properties, they usually diminish rapidly during the crystal growth process because of their high surface energies. To address this issue, organic polymers or inorganic ions have usually been employed for selective control of the growth rates of various crystal planes [2,5,7,12,15,18]. However, these capping agents adsorbed on the surfaces of semiconductor crystals generally reduce the catalytic activity as the result of decrease of the surface energy. Removal of the capping agents without surface reconstruction to maintain reactivity is still a great challenge.

Nickel oxide, a *p*-type semiconductor with a wide bandgap of 3.6–4.0 eV [19] is considered as one of the most perspective materials for lithium ion batteries [20], electrochemical supercapacitors [21], magnetics [22], gas sensors [23] and catalysis [24]. However, investigations on the photocatalytic behaviors of NiO are quite rare. Recently, the Cl^- ion capped NiO octahedrons with exposed {1 1 1} facets were found to have higher intrinsic photocatalytic activity than Degussa P25 TiO_2 particles [18]. Here, we report on the further activation of photocatalytic performance of the Cl^- ion capped NiO octahedron {1 1 1} facets by treatment of $AgNO_3$ and $NH_3{\cdot}H_2O$ solutions. The superior photocatalytic activities are attributed to clean {1 1 1} facets of the NiO octahedrons without Cl^- ions and the heterojunction between AgCl and NiO. The structure and atomic charge

* Corresponding author. Tel.: +86 029 81530710; fax: +86 029 81530702.
E-mail address: hqyang@snnu.edu.cn (H. Yang).

http://dx.doi.org/10.1016/j.apcatb.2015.02.007
0926-3373/Published by Elsevier B.V.

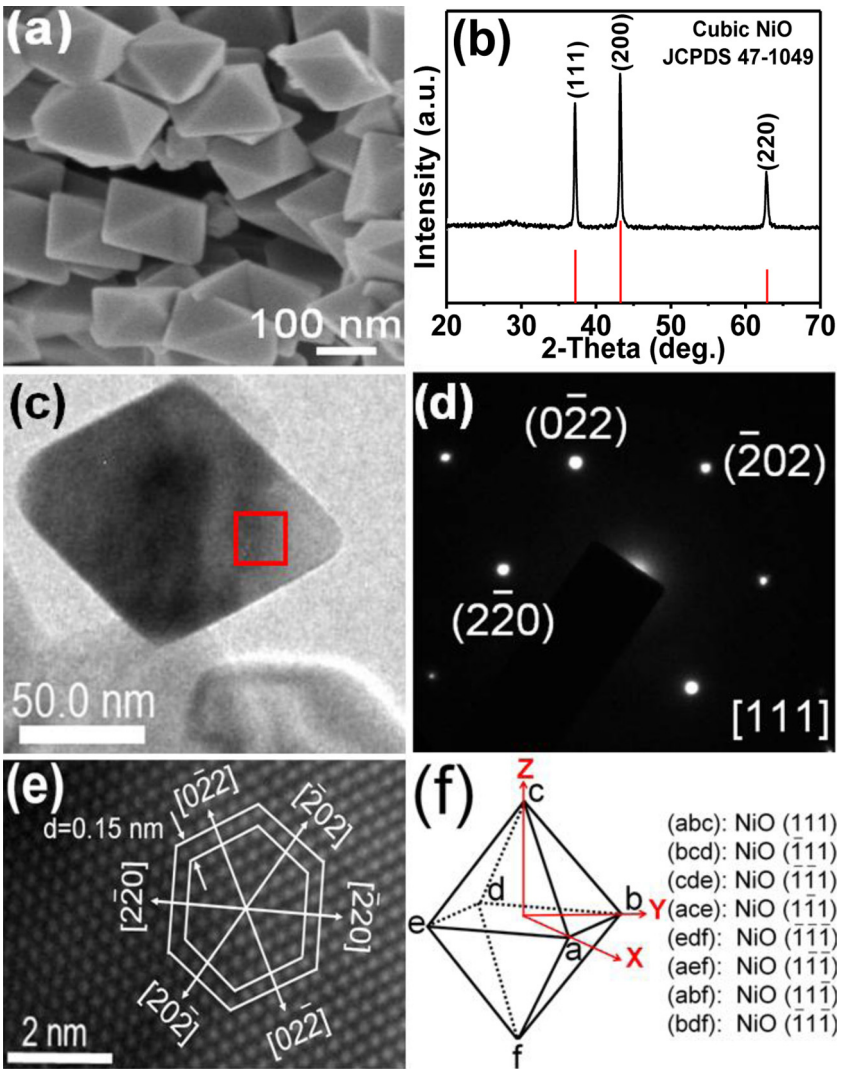

Fig. 1. (a) FESEM image and (b) XRD pattern of the-as synthesized octahedron structures. The stick pattern is the standard XRD pattern of cubic NiO powders with Cu Kα radiation (JPCDS card no. 47-1049). (c) TEM image of a single NiO octahedron. ((d) and (e)) SAED pattern and HRTEM image from the box in (c). (f) Crystal orientation of the NiO octahedron.

of the exposed NiO {1 1 1} facets are studied using periodic density functional theory (DFT). It is found that the exposed NiO {1 1 1} facets are polar surfaces. A charge separation model between polar {1 1 1} surfaces is proposed to explain the enhanced photocatalytic activities.

2. Experimental

2.1. Preparation

NiO octahedrons capped with Cl^- ions (Cl—NiO octahedrons) were prepared as follows: all reagents used were of analytical purity and were directly used without further purification. In a typical experiment, a silicon foil (1 × 1 cm) was cleaned in de-ionized water and absolute ethanol with ultrasonic irradiation for 15 min, respectively. One or two drops of 0.500 M $NiCl_2$ aqueous solutions were added on the silicon wafer in a quartz boat. The boat was positioned in a conventional box furnace. The furnace was heated to 400 °C at a rate of 20 °C/min and maintained at the temperatures for 1 h. After the furnace cooled down to room temperature, a large amount of gray products were obtained on the Si wafer.

Preparation of NiO octahedrons with loaded AgCl particles (AgCl—NiO octahedrons): In a typical process, 10 mg of the as-synthesized Cl—NiO octahedrons and 18.0, 26.0, 50.0, or 100.0 mL of 0.01 mol/L of $AgNO_3$ solution were put into a 200 mL beaker. The mixture was stirred for 30 min, then stands for 2 h in dark. The products were collected by centrifugation and then dried naturally in dark.

Preparation of AgCl particles: In a typical process, 5.0 mL of 1.0 mol/L $AgNO_3$ solution and 5.0 mL of 1.0 mol/L NaCl solution were added into a 50 mL beaker, the mixed solution then was stirred for 15 min to form a white precipitate. The white precipitate was collected by centrifugation and dried in dark at 60 °C.

2.2. Characterization

The as-prepared products were characterized and analyzed using powder X-ray diffraction (XRD), scanning electron microscopy (SEM), field emission scanning electron microscopy (FESEM) and transmission electron microscopy (TEM) and X-ray photoelectron spectra (XPS). The XRD analysis was performed using a DX-2700 X-ray diffractometer equipped with Cu $K\alpha_1$ radiation (λ = 1.541 Å) at 40 kV and 30 mA. Each specimen was scanned at a step size of 0.02° and a scanning speed of 8°/min with diffraction angles varying between 20 and 70°. SEM images were obtained using a FEI Quanta 200 scanning electron microscope at an

accelerating voltage of 20 kV. FESEM were obtained using a S-4800 field emission at an accelerating voltage of 3.0 kV. Energy-dispersive X-ray spectroscopy (EDX) facilities attached to the FESEM and SEM were employed to analyze chemical composition. TEM and electron diffraction images were obtained using a JEOL JEM-3010 TEM at an accelerating voltage of 300 kV. Samples for TEM were prepared by dispersing Cl—NiO and AgCl—NiO octahedron powders on a carbon-coated copper grid. XPS measurements were performed by using a Kratos Axis ultra X-ray photoelectron spectrometer with an excitation source of $Al_{K\alpha}$ = 1486.7 eV. The binding energies obtained in the XPS analysis were corrected for specimen charging through referencing the C1s to 284.6 eV. The Brunauer–Emmett–Teller (BET) specific surface area measurement was performed by N_2 gas adsorption using an America Micromeritics ASAP 2020 surface analytical instrument. The diffuse reflectance spectrum of the products was obtained on a Perkin Elmer Lambd 950 spectrophotometer.

The crystal structure of cubic NiO was calculated by using the DMOL3 code [25] and the generalized gradient approximation (GGA) with Perdew–Burke–Ernzerhof (PBE) functional is employed as the exchange-correlation functional [26]. The atomic charges are computed using Hirshfeld [27] population analyzes. The surface energy was computed using the formula [28]:

$$E_{\text{surface}} = \frac{E_{\text{slab}} - nE_{\text{bulk}}}{2A}$$

where E_{slab} is the total energy of the slab, E_{bulk} is the total energy of the bulk per unit cell, n is the number of bulk unit cells contained in the slab, and A is the surface area of each side of the slab, the 1/2 factor is used to obtain the average value of the surface energies of the top and bottom of the slab.

2.3. Evaluation of photocatalytic activity

Malachite Green (MG) with a molecular weight of 927, selected as model organic compounds to examine the photocatalytic activity of the AgCl—NiO octahedron structures, 10.0 mg of the as-prepared photocatalysts (samples 1–4) was added to 10.0 mL of 1.0×10^{-5} M MG solution to get a suspension. The suspension was magnetically stirred for 15 min in the dark to establish an adsorption/desorption equilibrium between the dye and the photocatalyst. The mixed solution was then irradiated with a 300 W medium-pressure mercury-vapor lamp at a distance of 8 cm (XPA-7 photochemical reactor, Xujiang Electromechanical Plant, Nanjing, China). At a given irradiation time interval, 5 mL of sample was withdrawn from the test tube for analysis. Sample solutions were obtained by centrifugation, and their absorption spectra were measured by on a U-2910 ultraviolet–visible spectrophotometer (HITACHI High-Technologies Corporation, Tokyo, Japan) using deionized water as reference. For comparison, the photocatalytic activities of Cl–NiO octahedrons, commercial TiO_2 (Degussa P25), AgCl particles and the mixture of Cl–NiO octahedrons and AgCl particles as well as NiO octahedrons with clean {1 1 1} faces were also tested under the same conditions and with the equal catalyst weight as that employed for AgCl–NiO octahedrons.

3. Results and discussion

3.1. Morphology and crystal structure of NiO octahedrons

NiO octahedrons capped with Cl^- ions were synthesized by heating $NiCl_2$ solution at 400 °C [18]. The as-obtained products were characterized and analyzed using powder FESEM, XRD and EDX. The FESEM observations (Fig. 1a) reveal that the products consist of a large quantity of octahedron structures with the edge lengths of 136–200 nm. The XRD pattern (Fig. 1b) and EDX spectrum

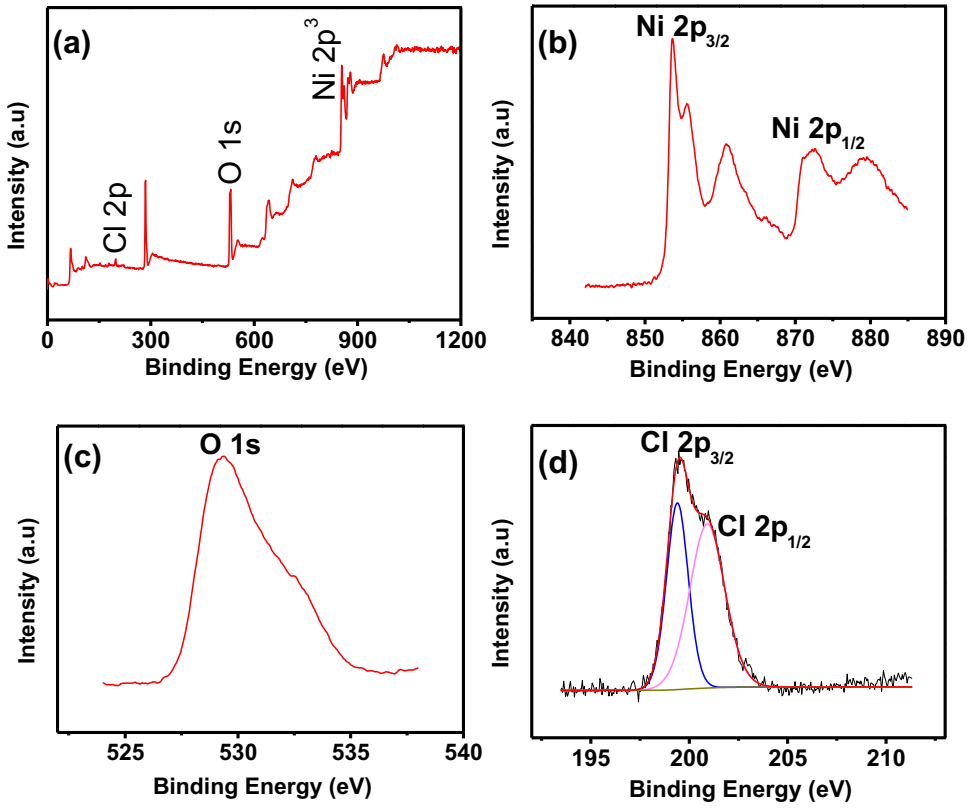

Fig. 2. XPS spectra of the-as synthesized Cl—NiO octahedron structures.

Table 1
NiO octahedrons with loaded cubic AgCl particles (AgCl—NiO octahedrons) obtained by the reaction of the Cl^- ion capped NiO octahedrons (Cl—NiO octahedrons) with various volumes of $AgNO_3$ solution.

Sample number	1	2	3	4
Weight of Cl—NiO octahedrons (mg)	10	10	10	10
Volume of $AgNO_3$ solution (mL)[a]	18	26	50	100

[a] Concentration of $AgNO_3$ solution is 1.0×10^{-2} mol/L.

(see Fig. S1) show that the as-synthesized octahedrons are cubic structured NiO crystals and there is a large quantity of Cl^- ions on the surface of the octahedrons. The selected area electron diffraction (SAED) pattern (Fig. 1d) and high-resolution TEM (HRTEM) image (Fig. 1e) from box in (Fig. 1c) indicate that the NiO octahedron is enclosed by (1 1 1), ($\bar{1}$ 1 1), ($\bar{1}$ $\bar{1}$ 1), (1 $\bar{1}$ 1), ($\bar{1}$ $\bar{1}$ $\bar{1}$), (1 $\bar{1}$ $\bar{1}$), (1 1 $\bar{1}$) and ($\bar{1}$ 1 $\bar{1}$) faces, and the schematic illustration of the crystal orientation is shown in Fig. 1f.

The XPS spectra of the as-prepared Cl–NiO octahedrons are shown in Fig. 2, including (a) the survey spectrum, (b) Ni $2p_{3/2}$ and $2p_{1/2}$, (c) O 1s, and (d) Cl $2p_{3/2}$ and $2p_{1/2}$. The binding energy of Ni $2p_{3/2}$ and $2p_{1/2}$ is identified at 852.8 and 870.2 eV, respectively (Fig. 2b). The peak at about 530.7 eV corresponds to O 1s, which is derived from NiO (Fig. 2c) [18,29]. The peaks at about 199.3 and 200.7 eV can be assigned to Cl $2p_{3/2}$ and $2p_{1/2}$, respectively (Fig. 2d) [18]. The XPS spectra and EDX analysis suggest that the formation of the NiO octahedrons may originate from the selective adsorption of Cl^- ions.

3.2. Morphology and crystal structure of AgCl–NiO octahedrons

Samples obtained by the reaction of the Cl^- ion capped NiO octahedrons with various volumes of $AgNO_3$ solutions were summarized in Table 1. FESEM images, EDX spectra and XRD patterns from samples 2 and 3 are shown in Figs. 3 and 4, respectively. The FESEM and XRD analysis indicate that the samples 2 and 3 consist of a large quantity of AgCl–NiO composite octahedrons with the edge lengths of 155–200 nm. There are some cubic structured AgCl nanoparticles with the sizes of 30–75 nm on the surface of the NiO octahedrons with the cubic structure. TEM images for sample 3 are shown in Fig. 5. We found that the sample is very sensitive to electron irradiation. The surface AgCl nanoparticles are so unstable that they are removed quickly from surface of the NiO octahedron under electron beam irradiation. The TEM observations reveal that the AgCl particles capped on the surface of the NiO octahedrons.

3.3. Formation mechanism of NiO octahedron structures

It is well known that NiO adopts the NaCl structure, with octahedral Ni^{2+} and O^{2-} sites, and its rock salt structure model is shown in Fig. 6a. The structure of (1 1 1) surface obtained from periodic DFT calculations is shown in Fig. 6b. It is clear that the (1 1 1) surface termination consists of a layer of unsaturated Ni sites, and all Ni atoms on the (1 1 1) plane are three-coordinated. In our system, Cl^- ions may serve as a ligand to Ni^{2+}, and adsorb selectively on unsaturated Ni sites on the NiO (1 1 1) surface. The most likely structure is described in Fig. 6c. The presence of Cl^- ions impedes the growth of the {1 1 1} surfaces. When the ratio of the growth rate in the <1 0 0> to that of the <1 1 1> equals to ~1.73, the perfect octahedrons are obtained [30].

3.4. Photocatalytic activity

The as-obtained AgCl particles were characterized by SEM and XRD. The results are shown in Fig. S2. It can be seen that the

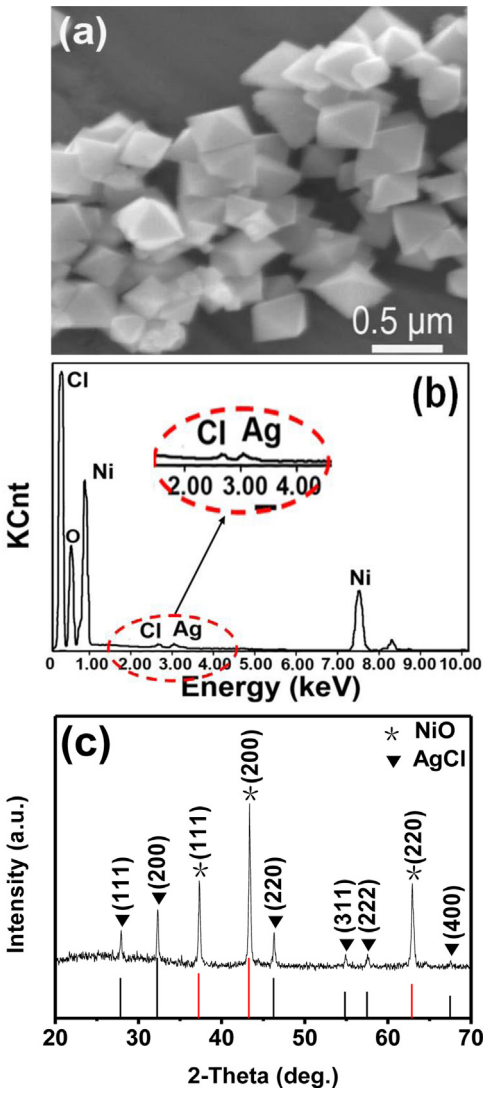

Fig. 3. (a) SEM image, (b) EDX spectrum and (c) XRD pattern of sample 2.

products consist of a large quantity of cubic AgCl particles with the sizes of 300–630 nm. To demonstrate the potential applicability in photocatalysis of the as-obtained AgCl loaded NiO octahedrons (AgCl—NiO octahedrons, samples 1–4), we investigated their photocatalytic activity by choosing photocatalytic degradation of MG as a reference, compared with Cl^- ion capped NiO octahedrons (Cl–NiO octahedrons) and Degussa P25 TiO_2 particles (P25). As shown in Fig. 7a, the decomposition of MG progresses slowly over Cl–NiO octahedrons (curve I) under mercury lamp irradiation. However, it decomposes more quickly in the presence of AgCl–NiO octahedrons (curves III–VI). The decomposition rates of samples 3 and 4 are almost the same, their decomposition rates are significantly larger than those for samples 1, 2, and P25 (curve II). In addition, we investigated photocatalytic activity of AgCl particles and the mixtures of AgCl particles and Cl–NiO octahedrons, compared with AgCl–NiO octahedrons (sample 3). As shown in Fig. 7b, the decomposition rate of MG over AgCl–NiO octahedrons is higher than that over AgCl particles, Cl–NiO octahedrons and the mixtures of AgCl particles and Cl–NiO octahedrons. The fittings of ln (C_0/C) plot vs. time over Cl—NiO octahedrons, AgCl particles, the mixture of AgCl particles and Cl—NiO octahedrons, P25 and samples 1, 2, and 3 are shown in Fig. 7c. The photodegradation of MG catalyzed by the seven kinds of catalysts can be explained using pseudo first-order reaction. i.e. ln (C_0/C) = kt, where k is the apparent rate

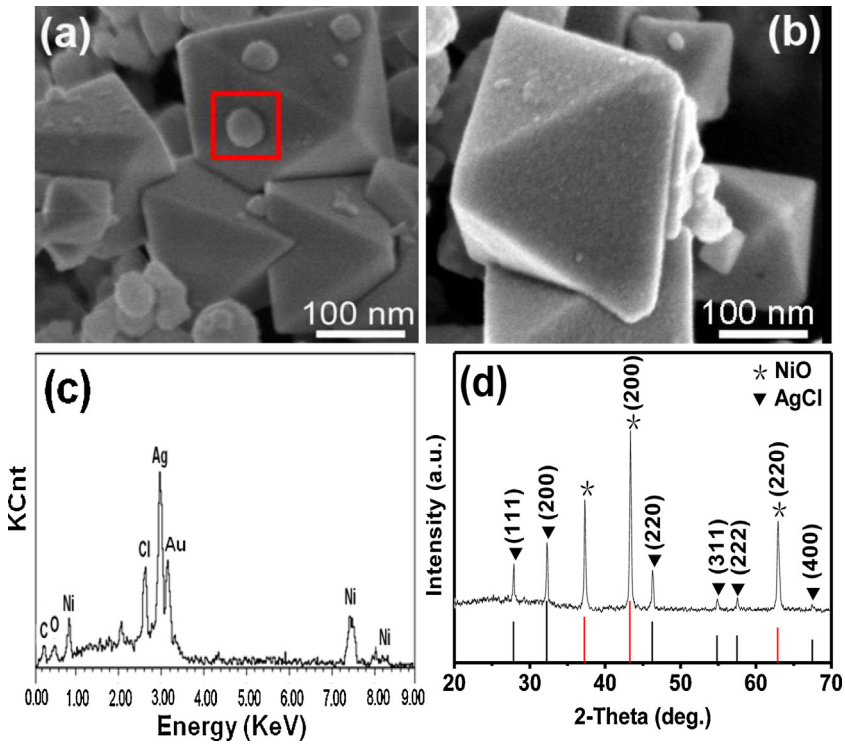

Fig. 4. ((a) and (b)) FESEM images of sample 3. (c) EDX spectrum from the box in (a). (d) XRD pattern of sample 3.

constant of the degradation. In our experiment, the k value is found to be 0.0072 ± 0.0002, 0.0095 ± 0.0005, 0.0192 ± 0.0004, 0.0635 ± 0.0013, 0.0963 ± 0.0018, 0.1490 ± 0.0053, and $0.2720 \pm 0.0100\ \mathrm{min}^{-1}$, respectively.

It is generally accepted that the catalytic process is mainly related to the absorption and desorption of molecules on the catalyst surface. The BET surface areas of Cl—NiO octahedrons, AgCl particles, the mixture of AgCl particles and Cl—NiO octahedrons, P25 and samples 1, 2, and 3 were measured, and the result is 25.38, 22.34, 18.92, 54.20, 15.00, 13.51, and $10.83\ \mathrm{m}^2\ \mathrm{g}^{-1}$, respectively. The apparent rate constant the degradation per unit surface area for the seven kinds of catalysts, as for the basis for the comparison, is examined in this work. It is found that values of the normalized k' for samples 1, 2, and 3 are larger than that for P25, Cl—NiO octahedrons, AgCl particles and the mixture of AgCl particles and Cl—NiO octahedrons, and the k' values for sample 3 is the highest, as shown in Fig. 7d and Table 2. The results indicate that the AgCl loaded NiO octahedrons exhibit higher photocatalytic activity than P25, Cl—NiO octahedrons, AgCl particles and the mixture of AgCl particles and Cl—NiO octahedrons, and its activity is enhanced with increasing volume of $AgNO_3$ solution. When the $AgNO_3$ solution volume is 50 mL, the photocatalytic activity reaches a saturated value. In addition, the diffuse reflectance spectra of the Cl—NiO octahedrons, the mixture of AgCl particles and Cl—NiO octahedrons as well as samples 1, 2, and 3 were measured. The results are shown in Fig. S3, apparently, change in the absorption spectra is small. Moreover, we investigated photocatalytic performance of the Cl^- ion capped NiO octahedrons treated by $NH_3{\cdot}H_2O$ solution, and the result is shown in Fig. 8a. It was found that the photocatalytic activity is also remarkably increased by $NH_3{\cdot}H_2O$ treatment. NiO octahedrons with clean {1 1 1} facets were prepared by the reaction of AgCl—NiO octahedrons (sample 3) with 3.0 mol/L $NH_3{\cdot}H_2O$ solution. The as-obtained products were characterized using FESEM, EDX and XRD, and the results are shown in Fig. S4. We clearly see that the as-obtained products consist of a large quantity of NiO octahedron structures. The exposed {1 1 1} facets of the NiO octahedrons are clean surfaces free of Cl^- ions or AgCl particles. We investigated photocatalytic activities of the NiO octahedrons with

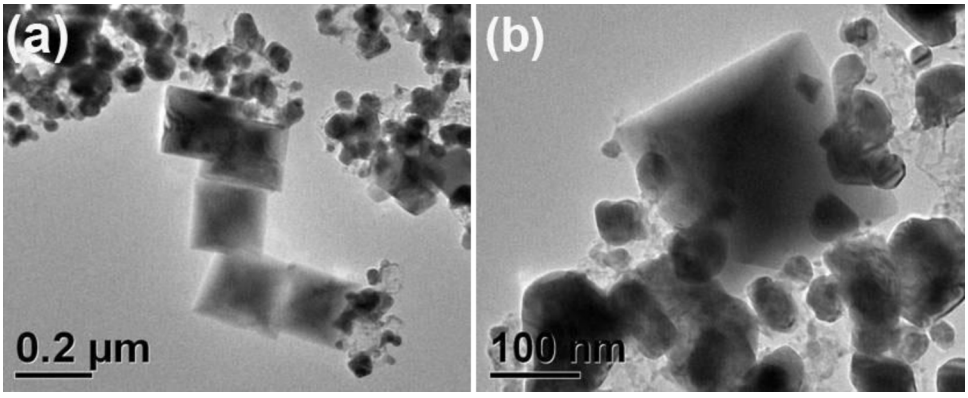

Fig. 5. TEM images of sample 3.

Table 2
BET specific surface area, k and k' of Cl—NiO octahedrons, AgCl particles, the mixture of AgCl particles and Cl—NiO octahedrons, P25 and samples 1, 2, and 3.

	Sample 1	Sample 2	Sample 3	AgCl + Cl—NiO[b]	AgCl	Cl—NiO	P25
Specific surface area ($m^{-2}\ g^{-1}$)	15.00	13.51	10.83	18.92	22.34	25.38	54.20
k (min^{-1})	0.0963 ± 0.0018	0.1490 ± 0.0053	0.2720 ± 0.0100	0.0192 ± 0.0004	0.0095 ± 0.0005	0.0072 ± 0.0002	0.0635 ± 0.0013
k' ($min^{-1}\ m^{-2}$)[a]	0.6420	1.1028	2.5185	0.1015	0.0425	0.0286	0.1171

[a] k': normalized apparent rate constant of the degradation per unit surface.
[b] AgCl + Cl—NiO: the mixtures of 1.0 mg of AgCl particles and 9.0 mg of Cl—NiO octahedrons.

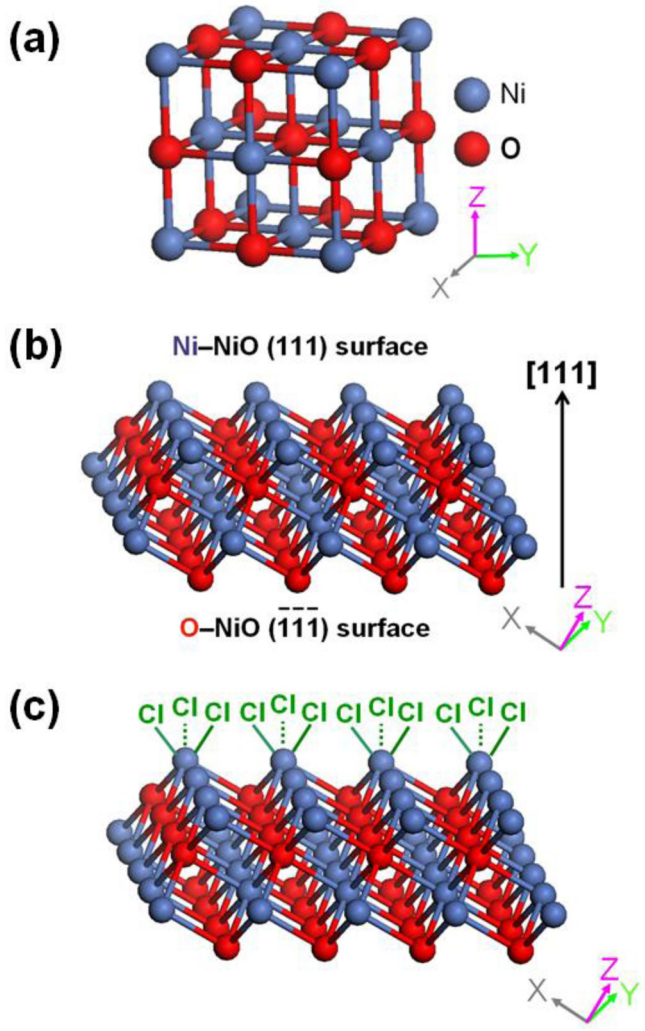

Fig. 6. (a) The cubic NiO crystal structure. (b) The atomic structures of (1 1 1) surfaces obtained from periodic DFT calculations. (c) The structure of the Cl^- ions attached to unsaturated Ni^{2+} sites on the (1 1 1) prismatic faces.

clean {1 1 1} facets, and compared with sample 3 and Cl—NiO octahedrons, and the results are shown in Fig. 8b. It apparently shows that the NiO octahedrons with clean {1 1 1} facets show higher photocatalytic activity than Cl—NiO octahedrons, but lower than sample 3. We therefore believe that the enhanced photocatalytic activities of the AgCl—NiO octahedrons may result from the removal of the surface Cl^- ions and loading of AgCl.

3.5. Charge separation between polar NiO {1 1 1} surfaces and photocatalysis mechanism

Surface energy of NiO (1 1 1), (2 0 0) and (2 2 0) surfaces was calculated using DFT. It is found that NiO (1 1 1) facet has much higher surface energy, 2.47, comparing to 0.97 for (2 0 0) and 1.50 J/m^2 for (2 2 0) facets, indicating that the {1 1 1} facets may show higher reactivity than {2 0 0} and {2 2 0} facets. The structure of (2 0 0) and (2 2 0) surfaces obtained from periodic DFT calculations is shown in Fig. 9. It is clear that the (2 0 0) and (2 2 0) faces are nonpolar surfaces, which is terminated with Ni and O atoms. However, the {1 1 1} facets are polar surfaces, they include a positive polar (1 1 1) plane terminated with Ni atoms, and a negative polar $(\bar{1}\bar{1}\bar{1})$ plane terminated with O atoms, as shown in Fig. 6b. On the basis of the above experimental results and theory analysis, we conclude that the clean NiO {1 1 1} facets are highly reactivity facets. Moreover,

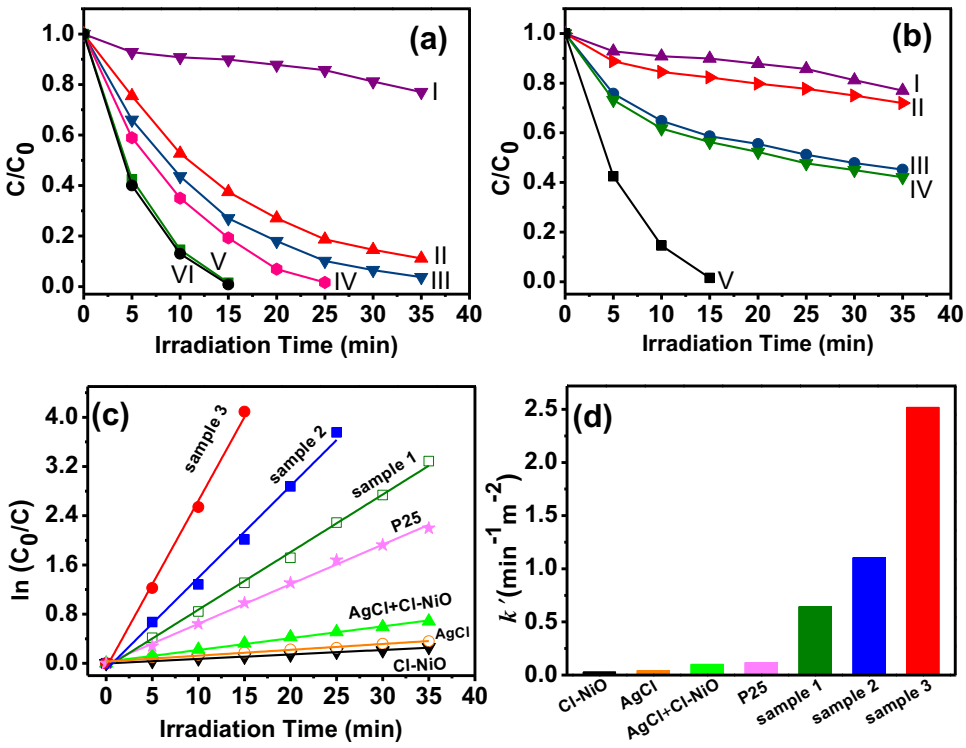

Fig. 7. (a) Photodegradation of the MG over Cl—NiO (I), P25 (II) and samples 1 (III), 2 (IV), 3 (V), and 4 (VI) under mercury lamp irradiation. (b) Photodegradation of the MG over Cl—NiO (I), AgCl (II), the mixture of 9.5 mg of Cl—NiO and 0.5 mg of AgCl (III), the mixture of 9.0 mg of Cl—NiO and 1.0 mg of AgCl (IV) as well as sample 3 (V) under mercury lamp irradiation. (c) The fitting of ln (C_0/C) plot vs. time over Cl—NiO, AgCl, the mixture of 0.1 mg of AgCl and 9.0 mg of Cl—NiO, P25 and samples 1, 2, and 3. (d) Normalized apparent rate constant (k') of the degradation per unit surface area over Cl—NiO, AgCl, the mixture of 9.0 mg of Cl—NiO and 1.0 mg of AgCl, P25 and samples 1, 2, and 3.

the heterojunction between AgCl and NiO contributes to increase in the photocatalytic activity.

For the NiO octahedron structures, the exposed {1 1 1} facets consist of four pairs of polar surfaces, as shown in Figs. Fig. 11f and Fig. 66b. Atomic charge distribution of the polar {1 1 1} surfaces obtained from periodic DFT calculations is shown in Fig. 10a. Each layer contains all positive Ni^{2+} ions or all negative O^{2-} ions in the [1 1 1] direction and the polar chain is shown in Fig. 10b. Charge of each Ni atom on the Ni—NiO (1 1 1) surface is +0.10 and O on the O—NiO ($\bar{1}\ \bar{1}\ \bar{1}$) surface is −0.13. The charge-centers of cations and anions separate and result in an electric dipole. An internal electric field thus is established between each pair of Ni–NiO and O–NiO planes by the spontaneous polarization. A charge separation model between polar {1 1 1} surfaces is thus proposed to explain the enhanced photocatalytic activities.

When the NiO octahedrons with exposed {1 1 1} polar facets were employed as a photocatalyst, the ultraviolet light irradiation induces a transition of electrons from the valence-band to the conduction-band, leaving an equal number of vacant sites (holes), and thus electron-hole pairs were formed in NiO octahedron (Eq. (1)) [31]. The photogenerated electrons and holes migrate to positive polar Ni—NiO (1 1 1), ($\bar{1}$ 1 1), (1 $\bar{1}$ 1) and (1 1 $\bar{1}$) and negative polar O—NiO ($\bar{1}\ \bar{1}\ \bar{1}$), (1 $\bar{1}\ \bar{1}$) (1 1 $\bar{1}$) and ($\bar{1}$ 1 $\bar{1}$) surfaces, respectively, under the internal electric field (Fig. 10c). The electrons on the positive polar Ni—NiO (111), ($\bar{1}$ 1 1), ($\bar{1}\bar{1}$ 1) and (1 $\bar{1}$ 1) surfaces are usually scavenged by O_2 to yield superoxide radical anions $O_2^{\bullet-}$ (Eq. (2)) [32]. The holes on the negative O—NiO ($\bar{1}\ \bar{1}\ \bar{1}$), (1 $\bar{1}\ \bar{1}$) (1 1 $\bar{1}$) and ($\bar{1}$ 1 $\bar{1}$) surfaces can react with surface adsorbed H_2O to produce $^{\bullet}$OH radicals (Eq. (3)), the dye molecules then are oxidized into CO_2, H_2O and mineralization products by $^{\bullet}$OH radicals (Eq. (4)) [32,33].

$$NiO + h\nu \rightarrow NiO\ (e_{CB}^{-} + h_{VB}^{+}) \quad (1)$$

$$e_{CB}^{-} + O_2 \rightarrow O_2^{\bullet-} \quad (2)$$

$$h_{VB}^{+} + H_2O \rightarrow H^{+} + {}^{\bullet}OH \quad (3)$$

$$^{\bullet}OH + \text{dye} \rightarrow CO_2 + H_2O \text{ mineralization products} \quad (4)$$

The NiO octahedrons with exposed clean {1 1 1} polar facets show excellent photocatalytic performance due to the presence of the internal electric field between the Ni—NiO and O—NiO polar surfaces. However, when Cl^- ions are adsorbed selectively on unsaturated Ni sites of {1 1 1} surfaces of NiO octahedrons, the surface Cl atom is negatively charged with −0.16, as shown in Fig. 10d. The internal electric field reduces between the Ni—NiO and O—NiO planes, and thus the Cl^- ion capped NiO octahedrons show poor photocatalytic activities. When the Cl^- ion capped NiO octahedrons reacted with $NH_3{\cdot}H_2O$ solution, the surface Cl^- ions were replaced by NH_3 molecules due to the strong coordinating effect of NH_3. The internal electric field is enhanced because that negative charge of NH_3 molecule is less than that of Cl^- ion, and thus photocatalytic performance of the Cl^- ion capped NiO octahedrons is increased by $NH_3{\cdot}H_2O$ solution treatment.

When the surface Cl^- ions reacted with Ag^+ ions to form AgCl, Ni atoms on the Ni—NiO (1 1 1) planes show positive charge, the strong internal electric field between the {1 1 1} polar surfaces are renewed. At the same time a heterojunction was formed between AgCl and positive polar Ni—NiO facet. The heterojunction improves further the separation of photogenerated electrons and holes, like the *p*-type NiO/*n*-type ZnO [34], MoS_2/CdS [35] and α-Fe_2O_3/NiO [36] heterojunctions. The photogenerated electrons transfer further from the Ni—NiO facets of NiO to the surface of AgCl particles. The reduction and oxidation reactions selectively take place on the surfaces of AgCl particles and negative polar O—NiO surfaces, and thus AgCl—NiO octahedrons show the enhanced photocatalytic activities (see Fig. S5).

Moreover, we carried out the MG bleaching experiment repeatedly four times by using the sample 3 as a catalyst. As shown

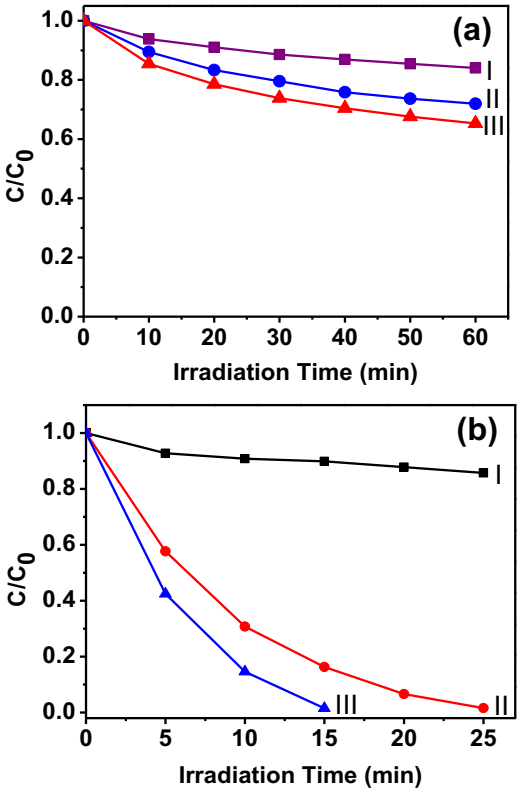

Fig. 8. (a) Photodegradation of the MG solutions over (I) Cl—NiO octahedrons, over (II) and (III) the Cl—NiO octahedrons treated by 25.0 mL of 1.0 and 2.0 mol/L $NH_3 \cdot H_2O$ solutions under mercury lamp irradiation. (b) Photodegradation of the MG solutions over Cl—NiO (I), NiO octahedrons with clean {1 1 1} facets (II) and sample 3 (III) under mercury lamp irradiation.

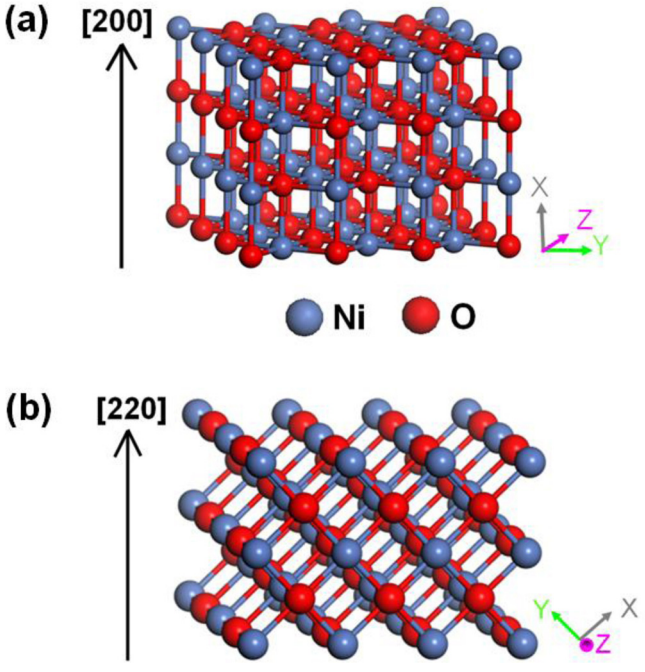

Fig. 9. ((a) and (b)) The atomic structures of (2 0 0) and (2 2 0) surfaces obtained from periodic DFT calculations.

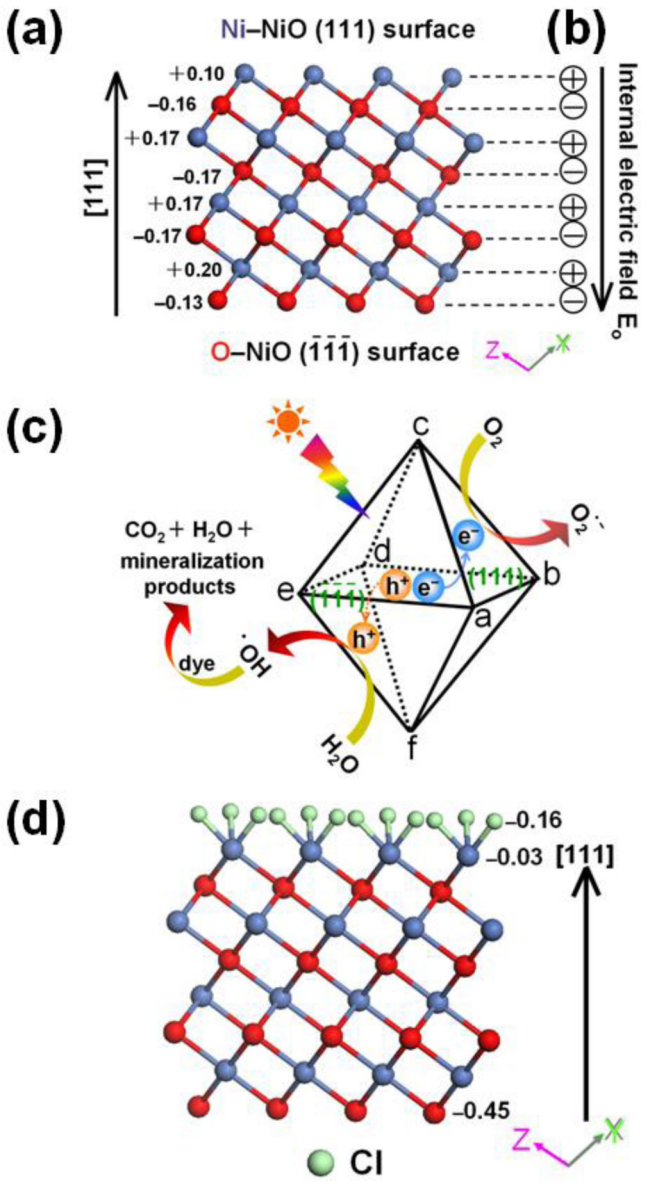

Fig. 10. (a) Atomic charge distribution of NiO (1 1 1) and ($\bar{1}\bar{1}\bar{1}$) faces obtained by DFT calculations. (b) The equivalent polar chain. (c) The schematic illustration of charge separation between polar {1 1 1} surfaces and photocatalytic reactions. (d) Atomic charge distribution of Cl^- ion capped (1 1 1) faces obtained by DFT calculations.

in Fig. 11, their photocatalytic activity was slightly lowered after four cycles, which indicated that the as-prepared AgCl—NiO octahedrons exhibit remarkable photocatalytic stability. After four cycles the sample 3 was characterized with FESEM, XRD and XPS, and the results are shown in Fig. S6. The FESEM and XRD observations indicate that after the photocatalytic test the products still consist of AgCl—NiO octahedron structures. A small quantity of AgCl particle was found to remove from surface of the NiO octahedron by comparing with SEM images of sample 3 in Fig. 4a. After the photocatalytic degradation experiment intensity of the NiO and AgCl diffraction peaks decreased, indicating its crystalline became poor. In the Ag 3d XPS spectrum, the two peaks centered at 367.52 and 373.57 eV can be attributed to Ag^+ (AgCl) instead of Ag^0 [37]. Moreover, the diffuse reflectance spectra of the sample 3 were measured before and after four cycles, and the results are shown in Fig. S7. It is found that after the photocatalytic degradation experiment, the diffuse reflectance spectrum of AgCl—NiO octahedron (sample 3) hardly changed. The results suggest that the decrease in the photo-

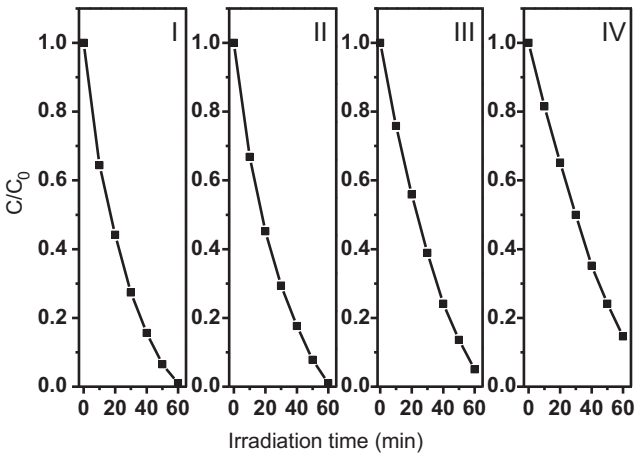

Fig. 11. Cyclic photodegradation of the MG solution with sample 3 under under mercury lamp irradiation.

catalytic activity may result from the removal of AgCl and the fall in NiO and AgCl crystalline.

4. Conclusions

Photocatalytic performance of the Cl^- ion capped NiO octahedrons with exposed {1 1 1} facets was activated by treatment of $AgNO_3$ and $NH_3{\cdot}H_2O$ solutions in this work. The superior photocatalytic activities are attributed to clean {1 1 1} facets of the NiO octahedrons free of Cl^- ions and the heterojunction between AgCl and NiO. Based on the polar structure of the NiO {1 1 1} surfaces, a charge separation model between polar {1 1 1} surfaces is proposed. Our results demonstrate that it is feasible to increase photocatalytic property of cubic structured NiO by selectively exposing the polar {1 1 1} facets. In addition, we may design and fabricate more effective photocatalysts and new type of photoelectrodes, solar cells, or photoelectric devices by the surface-engineering strategy.

Acknowledgements

This work was supported by the National Natural Science Foundation of China (Grant No. 21073116), the Natural Science Foundation of Shaanxi Province (Grant No. 2013JZ002) and the Fundamental Research Funds for the Central Universities (Grant Nos. GK201101004 and GK201402019).

Appendix A. Supplementary data

Supplementary data associated with this article can be found, in the online version, at http://dx.doi.org/10.1016/j.apcatb.2015.02.007.

References

[1] A. Fujishima, K. Honda, Nature 238 (1972) 37–38.
[2] H. Tong, S.X. Ouyang, Y.P. Bi, M. Oshikiri, N. Umezawa, M. Oshikiri, J.H. Ye, Adv. Mater. 24 (2012) 229–251.
[3] M.R. Hoffmann, S.T. Martin, W.Y. Choi, D.W. Bahnemann, Chem. Rev. 95 (1995) 69–96.
[4] J.H. Yang, D.G. Wang, H.X. Han, C. Li, Acc. Chem. Res. 46 (2013) 1900–1909.
[5] K.B. Zhou, Y.D. Li, Angew. Chem. Int. Ed. 51 (2012) 602–613.
[6] G. Liu, J.C. Yu, G.Q. Lu, H.M. Cheng, Chem. Commun. 47 (2011) 6763–6783.
[7] H.G. Yang, G. Liu, S.Z. Qiao, C.H. Sun, Y.G. Jin, S.C. Smith, J. Zou, H.M. Cheng, G.Q. Lu, J. Am. Chem. Soc. 131 (2009) 4078–4083.
[8] G.C. Xi, J.H. Ye, Chem. Commun. 46 (2010) 1893–1895.
[9] J. Jiang, K. Zhao, X.Y. Xiao, L.Z. Zhang, J. Am. Chem. Soc. 134 (2012) 4473–4476.
[10] D.Q. Zhang, S.L. Wang, J. Zhu, H.X. Li, Y.F. Lu, Appl. Catal. B 123 (2012) 398–404.
[11] H. Liu, M. Luo, J.C. Hu, T.F. Zhou, R. Chen, J.L. Li, Appl. Catal. B 140 (2013) 141–150.
[12] R. Jin, M.Y. Su, J. Wang, P. Zhang, M. Cui, Y. Chen, H.Q. Yang, Mater. Res. Bull. 47 (2012) 3070–3077.
[13] Y. Zhou, Z.P. Tian, Z.Y. Zhao, Q. Liu, J.H. Kou, X.Y. Chen, J. Gao, S.C. Yan, Z.G. Zou, ACS Appl. Mater. Interfaces 3 (2011) 3594–3601.
[14] Y.P. Bi, S.X. Ouyang, N. Umezawa, J.Y. Cao, J.H. Ye, J. Am. Chem. Soc. 133 (2011) 6490–6492.
[15] H. Zhao, W.Y. Yin, M.Y. Zhao, Y.Z. Song, H.Q. Yang, Appl. Catal. B 130 (2013) 178–186.
[16] Z.K. Zheng, B.B. Huang, Z.Y. Wang, M. Guo, X.Y. Qin, X.Y. Zhang, P. Wang, Y. Dai, J. Phys. Chem. C 113 (2009) 14448–14453.
[17] S.D. Sun, X.P. Song, Y.X. Sun, D.C. Deng, Z.M. Yang, Catal. Sci. Technol. 2 (2012) 925–930.
[18] B. Liu, A.H. Wei, J.Y. Zhang, L.J. An, Q.Q. Zhang, H.Q. Yang, J. Alloys Compd. 544 (2012) 55–61.
[19] L. Xu, R.F. Zheng, S.H. Liu, J. Song, J.S. Chen, B. Dong, H.W. Song, Inorg. Chem. 51 (2012) 7733–7740.
[20] G.M. Zhou, D.W. Wang, L.C. Yin, N. Li, F. Li, H.M. Cheng, ACS Nano 6 (2012) 3214–3223.
[21] S. Vijayakumar, S. Nagamuthu, G. Muralidharan, ACS Appl. Mater. Interfaces 5 (2013) 2188–2196.
[22] J.Y. Song, C.H. Kim, J.H. Cho, Y.H. Shin, H.M. Jang, ACS Nano 4 (2010) 3288–3292.
[23] B. Liu, H.Q. Yang, H. Zhao, L.J. An, L.H. Zhang, R.Y. Shi, L. Wang, L. Bao, Y. Chen, Sens. Actuators B 156 (2011) 251–262.
[24] Y.P. Wang, J.W. Zhu, X.J. Yang, L.D. Lu, X. Wang, Thermochim. Acta 437 (2005) 106–109.
[25] B. Delley, J. Chem. Phys. 92 (1990) 508–517.
[26] J.P. Perdew, K. Burke, M.G. Ernzerhof, Phys. Rev. Lett. 77 (1996) 3865–3868.
[27] F.L. Hirshfeld, Theor. Chim. Acta 44 (1977) 129–138.
[28] J.C. Boettger, Phys. Rev. B 49 (1994) 16798–16800.
[29] S. Uhlenbrock, C. Scharfschwerdt, M. Neumann, G. Illing, H. Freund, J. Phys. Condens. Matter 4 (1992) 7973–7978.
[30] Z.L. Wang, J. Phys. Chem. B 104 (2000) 1153–1175.
[31] M.R. Hoffmann, S.T. Martin, W. Choi, D.W. Bahneman, Chem. Rev. 95 (1995) 69–96.
[32] C.C. Chen, W.H. Ma, J.C. Zhao, Chem. Soc. Rev. 39 (2010) 4206–4219.
[33] N. Sobana, M. Swaminathan, Sep. Purif. Technol. 56 (2007) 101–107.
[34] Z.Y. Zhang, C.L. Shao, X.H. Li, C.H. Wang, M.Y. Zhang, Y.C. Liu, ACS Appl. Mater. Interfaces 2 (2010) 2915–2923.
[35] X. Zong, H.J. Yan, G.P. Wu, G.J. Ma, F.Y. Wen, L. Wang, C. Li, J. Am. Chem. Soc. 130 (2008) 7176–7177.
[36] Y. Jiao, Y. Liu, B.S. Yin, S.W. Zhang, F.Y. Qu, X. Wu, Nano Energy 10 (2014) 90–98.
[37] R.F. Dong, B.Z. Tian, C.Y. Zeng, T.Y. Li, T.T. Wang, J.L. Zhang, J. Phys. Chem. C 117 (2013) 213–220.